Femtosecond probing of photodissociation dynamics in acyl cyanides

I-Ren Lee, Yu-Chieh Chung, Wei-Kan Chen, Xiu-Ping Hong, and Po-Yuan Cheng[a)]
Department of Chemistry, National Tsing Hua University, Hsinchu, Taiwan, Republic of China

(Received 13 June 2001; accepted 24 September 2001)

The photodissociation of two acyl cyanide compounds, R–C(O)–CN, where R=methyl and tert-butyl groups, has been investigated using femtosecond time-resolved laser-induced fluorescence (LIF) spectroscopy. Both compounds were excited by two-photon excitation at a total energy of ~6.4 eV and the formation of the free CN(X) radical products was probed in real time by monitoring the CN $X \rightarrow B$ LIF signal. The results revealed that the temporal evolution of the CN(X) formation can be well characterized by delayed biexponential rise functions with time constants in the picosecond time scale, indicating that the dissociation occurs via a complex-mode mechanism. We proposed a dissociation mechanism involving two discernable stages to account for the observed temporal behaviors as well as previous photofragment translational spectroscopic results reported by other groups. Our analyses suggested that the selectivity between the C–CN and C–R bond cleavage is determined by the competition between the adiabatic and nonadiabatic dynamics of the S_2 state. The results also indicated that the adiabatic dissociation process occurring on the S_2 surface is not statistical. We speculate that this nonstatistical dissociation behavior is due to an initial nonuniform phase space distribution and a slow intramolecular vibrational energy redistribution process that prevents the system from sampling the entire phase space before the reaction completes.
 [DOI: 10.1063/1.1418250]

I. INTRODUCTION

The Norrish type-I reaction in asymmetrically substituted carbonyl compounds has attracted great research interest for many years.[1–10] The major focuses have been to measure the branching ratio between the two nonequivalent α-bond dissociation channels upon electronic excitation and to reveal the underlying mechanisms that may provide important implications to the ''bond-selective chemistry.'' In asymmetrically substituted aliphatic ketones the weaker α-C–C bond has generally been found to break preferentially at low excitation energies.[1–3] It is believed that this α-C–C cleavage occurs on the $^3(n,\pi^*)_{CO}$ surface over a barrier due to an avoided crossing with the higher lying repulsive surface $^3(\sigma,\sigma^*)_{CC}$.[1–3] Since the latter dissociates to the ground state products, the barrier heights usually correlate with the α-C–C bond energies. Consequently, the weaker α-C–C bond is cleaved preferentially if the reaction is statistical. On the other hand, very different branching behaviors have been observed for nonalkyl substituted carbonyls. For example, it was observed that the C–Cl bond cleaves preferentially over the C–C bond in acetyl chloride, despite the near equivalence of the two α-bond energies.[6–8] The nonstatistical branching is even more pronounced for acetic acid in which the OH elimination is strongly favored over CH_3 elimination even though the C–OH bond is stronger than the C–CH_3 bond.[9,10] In the case of acetyl chloride, Butler's group[6–8] has pointed out that the selectivity arises from the fast C–Cl bond dissociation occurring on the initially excited adiabatic potential energy surface formed via the interaction between the $^1(n,\pi^*)_{CO}$ and $^1(n_{Cl},\sigma^*_{C-Cl})$ diabates, whereas the C–CH_3 fission has to occur on the $^3(n,\pi^*)_{CO}$ surface reached via the much slower intersystem crossing. It is clear that the nonalkyl substituents in these compounds give rise to new photochemical pathways that are not present in their aliphatic counterparts and significantly alter the reaction branching.

Acetyl cyanide, $CH_3(CO)CN$, is another simple carbonyl compound that possesses many similar appealing properties. First, the C–CN bond is much stronger than the C–CH_3 bond because a partial conjugation between the CO and CN groups is present. Secondly, the unsaturated substituent (–CN) could give rise to low-lying electronic excited states leading to new photochemical pathways. In addition, the –CN group is usually considered as a ''pseudohalogen,'' and it is intriguing to compare the photochemistry of acetyl cyanide with the well-studied acetyl chloride.[6–8] Accordingly, The photodissociation of acetyl cyanide has attracted a great deal of research attention in recent years and has been studied by several groups using a variety of techniques.[11–14]

Upon excitation of acetyl cyanide to high enough energy, cleavage of either nonequivalent α-C–C bonds can occur,

$$CH_3C(O)CN \rightarrow CH_3CO + CN, \quad (1)$$

$$CH_3C(O)CN \rightarrow CH_3 + OCCN. \quad (2)$$

The bond dissociation energies of the two α-bonds have been estimated to be D_0(C–CN)=427 kJ/mol and D_0(C–CH_3) =359 kJ/mol on the bases of *ab initio* calculations and thermochemical data.[11,15] The much stronger C–CN bond clearly suggests a partial conjugation between the CO and CN moi-

a)Author to whom correspondence should be addressed. Electronic mail: pycheng@mx.nthu.edu.tw

eties, as expected. If sufficient energy is partitioned into the internal degrees of freedom of the photofragments, secondary dissociation may subsequently occur,

$$CH_3CO \rightarrow CH_3 + CO, \tag{1a}$$

$$COCN \rightarrow CO + CN. \tag{2a}$$

Horwitz *et al.*[11] probed the energy distributions of the CN(X) fragments arising from photodissociation of acetyl cyanide at 193 nm using laser-induced fluorescence. They found that CN(X) fragments are produced with rotational and vibrational distributions that can be described by Boltzmann distributions at a temperature of ~1800 K. Evidences were presented in their report to conclude that the majority of CN(X) fragments are produced via the primary C–CN cleavage, i.e., reaction (1).[11]

North *et al.*[12] also studied photodissociation of acetyl cyanide at 193 nm using high-resolution transient frequency modulation spectroscopy and photofragment translational spectroscopy. The rotational and vibrational distributions of the CN(X) fragments were found to be similar to those reported by Horwitz *et al.* However, the mean translational energy of CN was determined to be 19.0 ± 0.6 kJ/mol, much lower than the previously reported value.[11] The anisotropy for the CN photofragments was found to be very low, suggesting that the dissociation is not due to a direct dissociation. These combined measurements led them to conclude that there is a strong preference for primary CN elimination (1) over the CH_3 elimination (2), despite a large difference in the two α-C–C bond energies.[12]

Owrutsky and Baronavski[14] studied the photodissociation of acetyl cyanide at 193 nm using femtosecond mass-resolved multiphoton ionization spectroscopy. They observed a pulse width limited decay (<200 fs) from monitoring the parent mass channel. When the acetyl radical mass channel was monitored, a decay of 390 fs was observed. They ascribed the ultrafast parent decay to the short lifetime of the initially excited state, which they presumed to be a manifestation of a prompt dissociation (<200 fs). They have also performed *ab initio* calculations to assign the relevant electronic excited states. They argued that the isotropic photofragment distribution observed by North *et al.*[12] is not a result of a slow dissociation; rather it is due to the angle between the transition dipole moment and the dissociating C–C bond being close to the magic angle (54.7°).[14]

Recently, Furlan *et al.*[13] reinvestigated the photodissociation of acetyl cyanide at 193 nm using photofragment translation spectroscopy (PTS). In contrast to the previous report,[12] they did observe products arising from the primary CH_3 elimination reaction (2). They concluded that the CN elimination channel is still the major one and represents a branching of $85 \pm 10\%$, whereas the CH_3 elimination channel has a branching of only $15 \pm 10\%$.[13] The translational energy distribution for the primary CN elimination channel was found to peak at a very low energy with a mean value of 10 ± 2 kJ/mol, which is compatible only with the formation of CH_3CO or CN in one of the energetically accessible electronically excited states. Using the measured ratio of the stable and unstable CH_3CO counterfragments they estimated that about 91% of the CN elimination leads to the formation of "$CN(A) + CH_3CO(\tilde{X})$" and/or "$CN(X) + CH_3CO(\tilde{A})$," whereas the remaining 9% leads to the all-ground-state products. In addition to acetyl cyanide, Furlan *et al.*[13] also studied a series of related cyano carbonyl compounds X–C(O)CN, with X=isopropyl, tert-butyl, and methoxy groups. The mean translational energies released for the primary CN elimination channel in these compounds were found to be much higher. They also concluded that the secondary dissociation of the OCCN radical to "CN+CO" is unimportant ($\leqslant 5\%$) for all the X–C(O)CN compounds they have studied.[13] More interestingly, the branching for the primary CN elimination decreases from $85 \pm 10\%$ for acetyl cyanide to $30 \pm 10\%$ for isobutyryl cyanide (X=isopropyl), $17 \pm 10\%$ for pivaloyl cyanide (X=tert-butyl), and $5 \pm 2\%$ for methyl cyanoformate (X=methoxy).[13] Thus, the propensity for C–CN α-cleavage is lost with increasing size of the alkyl group. They suggested that the formation of electronically excited CN and/or acetyl radicals in the CN elimination channel might be responsible for the preferred C–CN bond breaking in acetyl cyanide.

In spite of the recent efforts described above, there still remain questions regarding the time scales and mechanism involved in the photodissociation of acetyl cyanide. In this work, we studied the photodissociation of two acyl cyanide compounds, R–C(O)–CN, where R=CH_3 for acetyl cyanide and R=$C(CH_3)_3$ for pivaloyl cyanide, using femtosecond (fs) pump–probe laser-induced fluorescence (LIF) spectroscopy. Figure 1 shows the chemical structures of the two compounds and illustrates the methodology employed in this work. Both compounds were excited by fs laser pulses through a two-photon transition at ~388 nm to the similar energy region reached by the 193 nm one-photon excitation. The temporal evolution of the CN(X) products formation was then probed in real time by monitoring the CN $X \rightarrow B$ LIF signal using a second delayed fs pulse also at 388 nm. Owing to their low molecular symmetries, transitions from the electronically ground state to any excited states are both one- and two-photon allowed. Thus, since the total excitation energies are nearly identical, the initial states accessed by the present two-photon excitation at 388 nm should be the same as those reached by one-photon excitation at 193 nm employed in previous studies. A unique feature of this work is the resonance probing of the free CN(X) products, which ensures definite identification of the reaction products. This approach is essentially the same as that devised by the Zewail's group many years ago in their first ICN fs clocking experiment.[16] Our results revealed that the CN(X) photofragments are produced through two very different temporal processes, providing important complementary information to the previous results.[11–14] In our previous report on this subject,[17] we have focused on the nonstatistical behavior for the photodissociation of these two acyl cyanide compounds. Here, we will focus on the elucidation of dissociation mechanism and the bond breakage selectivity.

II. EXPERIMENT

The fs laser system employed in this work consisted of a self-mode-locked Ti:sapphire laser (Spectra Physics, Tsu-

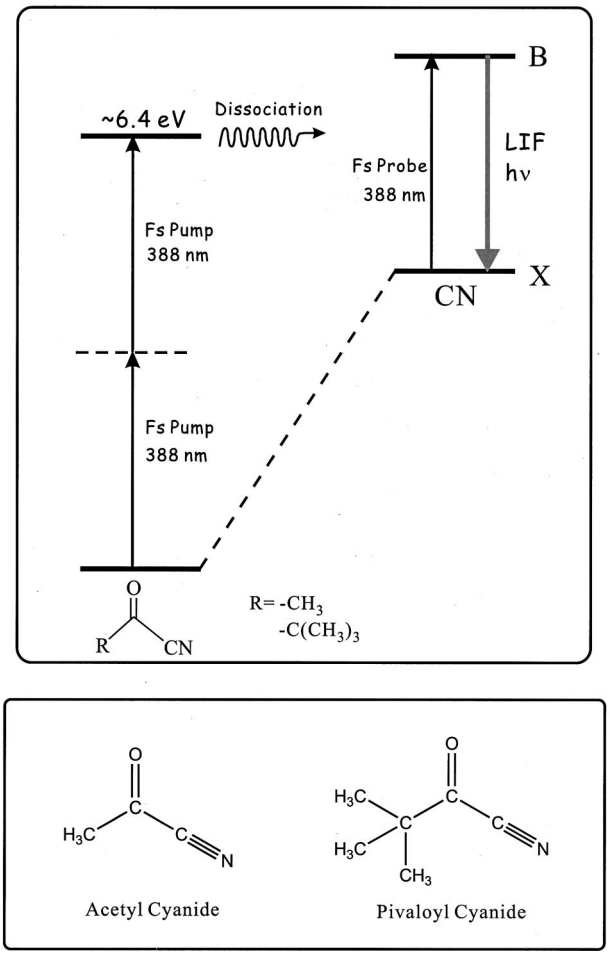

FIG. 1. Upper panel: Schematic diagram showing the pumping and probing schemes employed in this work. Note that at the one-photon excitation level, it is not energetically possible to eliminate CN from both compounds. Lower panel: The chemical structures of the two compounds studied in this work.

nami) and a chirp-pulse regenerative amplifier (''CPA,'' Spectra Physics, Spitfire). The oscillator produced 82 MHz, ~80 fs pulse trains with an average power of ~1 W around 800 nm. To detect CN radicals, the oscillator output wavelength was tuned to around 776 nm. These pulses were selectively amplified through the stretcher, regenerative amplifier and compressor stages in the CPA, producing 1 kHz fs pulses of ~1 mJ/pulse in energy and ~120 fs FWHM in duration at ~776 nm. The CPA output was split into two parts by a 30/70 beamsplitter. The transmitted and reflected beams were both frequency-doubled in thin BBO crystals to produce fs pulses at ~388 nm. Since the pump and probe pulses are of the same wavelength, similar transient CN fluorescence signal can be observed in both directions with respect to the zero of time, if both beams are comparable in pulse energies. To avoid confusion, we placed neutral density filters in the beam paths to adjust the irradiance of both beams such that the pulses in one beam are much more intense than those in the other beam. In the following discussion, we will refer to the more intense pulses as the ''pump'' and the weaker ones the ''probe.'' For the transients presented here the probe laser was attenuated to about 10–20 times weaker than the pump laser, resulting in a negligible negative-time signal in comparison with the positive-time signal due to the two-photon pumping scheme employed here. The probe beam was sent through a retroreflector mounted on a computer-controlled translation stage. A polarizer was also placed in the probe beam path to set its polarization at the magic angle (54.7°) with respect to that of the pump in order to minimize any rotational coherence effect. The pump and probe beams were then collinearly recombined via a neutral density beamsplitter and focused into the gas cell through a $f=500$ mm lens. The typical pulse energies before entering the cell were ~10–20 μJ for the pump and ~0.5–1.0 μJ for the probe.

The gas cell, which is a hollowed stainless steel cube with two light-baffled arms, was continuously evacuated with a mechanical pump through a liquid-nitrogen trap and a molecular-sieve trap. Acetyl cyanide and pivaloyl cyanide (Aldrich, 96%) were subjected to several freeze–pump–thaw cycles and vacuum distillation prior to use. The vapor was slowly flowed into the cell through a needle valve to maintain a pressure of ~500 mTorr in the cell during the experiments. The laser beams passed the cell through several light baffles to reduce the scattered light level. The laser-induced fluorescence of CN fragments was collected at right angle to the direction of the laser beams through two f/1.5 plano-convex lens (2 in. diam.). The second lens focused the fluorescence through an aperture onto the photocathode of a photomultiplier tube (Hammamatsu, 1P27). A ~35 nm (FWHM) bandpass filter centered at 405 nm and a long-pass filter (380 nm cutoff) were placed in the light collection system to further reduce the scattered light and to ensure that only fluorescence photons in the 388–422 nm spectral region can be detected efficiently. The signal from the photomultiplier tube was amplified and then sent to a boxcar gate integrator for signal averaging. The gate was typically 100 ns in duration and was delayed from the laser pulse to avoid interference from the scattered light. The transients were obtained by monitoring the fluorescence signal while the pump vs probe delay time was scanned.

In addition to the experimental studies, we also carried out *ab initio* electronic structure calculations using the GAUSSIAN 94 (Ref. 18) and GAUSSIAN 98 (Ref. 19) programs to elucidate the nature of excited states involved and to obtain relevant molecular parameters. Computational methods will be described in the Discussion.

III. RESULTS AND ANALYSES

A. Acetyl cyanide

Upon excitation of acetyl cyanide vapor at ~388 nm, transient fluorescence was readily observed. Figure 2 shows the observed transients at three different time scales. We assigned this transient fluorescence signal to the free CN(X) fragments arising from acetyl cyanide photodissociation on the bases of following reasons: (1) the signal was at the maximum when the probe laser wavelength was set at the bandhead of the CN $X \rightarrow B(0,0)$ transition near 388 nm.[20] When the laser wavelength was tuned to spectral regions outside the expected CN $X \rightarrow B(0,0)$ rotational envelope for CN(X) produced at a rotational temperature of 1800 K,[11]

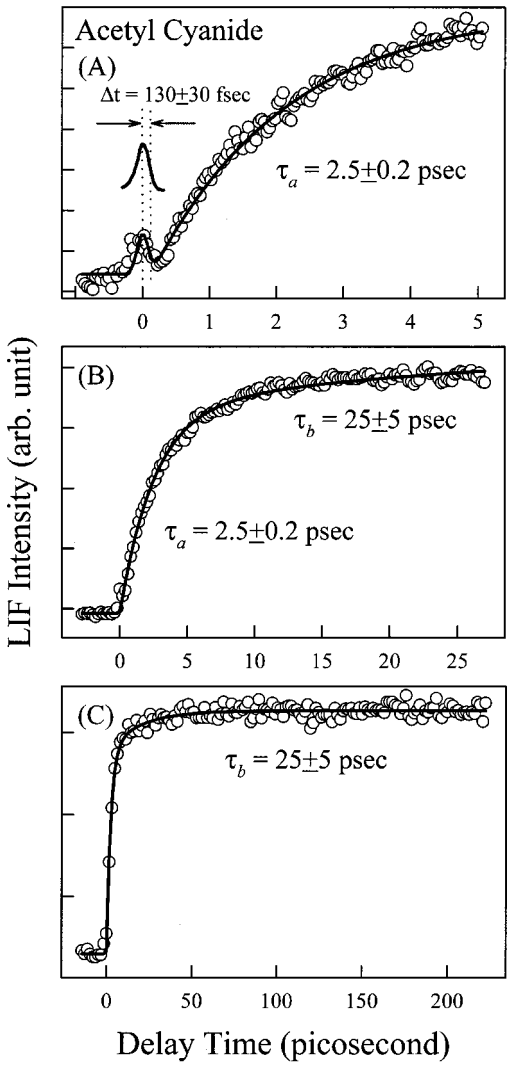

FIG. 2. CN(X) transients recorded by monitoring the CN $X \rightarrow B$ LIF signal as a function of the pump–probe delay time upon two-photon excitation of acetyl cyanide at 388 nm for three different time scales. The three transients have been normalized to the same maximum intensity. The open circles are the experimental data points and the solid lines are results of nonlinear least-squares fits to a sum of a delta function at the zero delay time and a delayed biexponential-rise function, both convoluted with a 200 fs FWHM Gaussian response function. A single set of time constants were used to obtain the best fits simultaneously for all three transients of different time scales. A cross-correlation trace is also shown in (A) for comparison. The time constants obtained from the fits are indicated in the figure and the amplitude ratio obtained from fitting the transient in (C) is $A_a:A_b=4.5:1$. The origins of the early-time features, i.e., the initial spike and the initial delay, are discussed in the text.

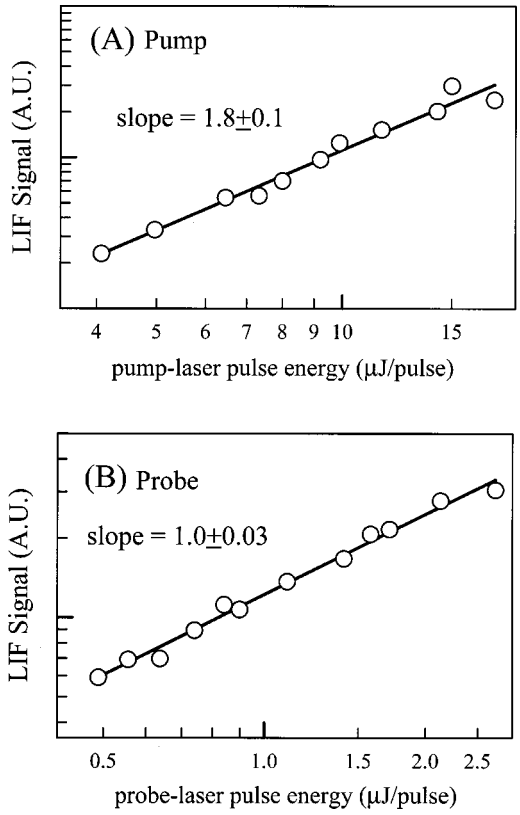

FIG. 3. (A) Pump- and (B) probe-laser irradiance dependencies of the transient CN(X) LIF signal arising from the photodissociation of acetyl cyanide. In these measurements, both beams were focused through a $f=500$ mm lens and the pulse widths were about 140 fs FWHM. We assumed the dependence of the transient signal (S) on the laser irradiance (I) follows $S=\sigma I^n$ (Ref. 23). The data points were plotted on a log–log scale and the slope of the best-fitted straight line gave the dependence exponent (n). Although these data were taken at a pump-probe delay time of ~1 ps, results obtained at longer times were found to be similar. Moreover, the shapes of the transients remained unchanged within the pulse energy ranges studied here.

e.g., at $\lambda_{probe}>390$ nm, no transient LIF signal was observed. (2) The spectral filters used in the light collection system allowed only photons in the CN $B \rightarrow X(0,0)$ fluorescence spectral region to enter the photomultiplier tube. (3) The probe-laser irradiance dependence of the LIF signal is nearly unity, as shown in Fig. 3(B), indicating a one-photon probing process. (4) The observed fluorescence lifetime is ~20 ns; shorter (not longer) than the literature value of 63 ns (Ref. 21) for the CN B state under collisionless conditions. The discrepancy is due to the relatively high pressure (~500 mTorr) of gas used here. In fact, it has been reported that the lifetime of the CN B state measured in a 700 mTorr BrCN vapor is 33 ns,[22] qualitatively consistent with our observation. The combined evidences presented above unambiguously indicate that the observed transient fluorescence is due to free CN(X) radicals produced from the acetyl cyanide photodissociation. The transient CN(X) signal rises to a constant maximum level and does not decay for the longest delay time available in our setup (~1.2 ns), indicating that the probe laser bandwidth is only broad enough to cover the dissociation asymptote region and that the observed transients truly reflect the formation dynamics of the free products.[16]

Since it is not energetically feasible for one 388 nm photon (308 kJ/mol) to eliminate CN from the two compounds, the observed CN fragments must be a consequence of multiphoton excitation. We have carried out pump-laser irradiance dependence measurements, shown in Fig. 3(A), and found that the dependence exponent of the transient CN LIF signal is $n=1.8\pm0.1$ (see caption of Fig. 3) around the typical pump-laser energy used here. This strongly suggests that a two-photon excitation is responsible for the observed transients. At higher laser irradiance attained by using a focusing lens with a shorter focal length of 200 mm, the pump-laser irradiance dependence became greater and a more intense

temporal feature with a shorter rise time of ~400 fs emerged. This new feature, which appeared only at high pump-laser irradiance, is probably due to a three-photon or even higher order excitation, reaching higher neutral or ionic states in which CN can be eliminated more rapidly. To avoid interference from these higher states, we have used a $f=500$ mm focusing lens and pump-pulse energies as low as possible for the data presented here. Within the pump-pulse energy range shown in Fig. 3, the shape of transients is independent of the pump-pulse energy and the irradiance dependence is close to 2. We therefore concluded that the CN transients shown in Fig. 2 is due to a two-photon excitation of acetyl cyanide at 388 nm. Hence, our initial excitation reached the similar energy region studied by other groups[11–14] using one-photon excitation at 193 nm.

A single-exponential fit to the early-time transient shown in Fig. 2(A) seemed to suggest that free CN fragments appear exponentially. However, careful examinations of the longer time scale transients shown in Figs. 2(B) and 2(C) revealed that there is a much slower and weaker temporal feature with a time constant of about 25 ps on top of the faster rise. Beyond ~100 ps the transient LIF signal stays at a constant level for up to the longest delay time of 1.2 ns limited by our translation stage. We have also tuned the pump and probe lasers to other wavelengths (386–389 nm) within the expected rovibronic envelope of the CN $X \rightarrow B(0,0)$ transitions at 1800 K (Ref. 11) and, except for an expected decrease in the signal size, we observed no significant wavelength dependence for the shape of the transients.

One also notes that there is a sharp temporal feature near the zero of time in the transient shown in Fig. 2(A). We have measured the pump- and probe-laser irradiance dependence of this spiking feature and found that they are greater than those of the subsequent biexponential rise. In fact, by making the pump and probe lasers much more intense, the initial spike can become much larger than the rise components. Under high irradiance conditions, we found that this sharp feature resembles the cross correlation trace of the pump and probe pulses in terms of the temporal width and position, as shown in Fig. 2(A). It thus serves as a convenient reference to the zero of time. We assigned this spiking feature to the enhanced multiphoton absorption occurring when two pulses overlap in time. These cooperative processes reach higher excited states of acetyl cyanide in which CN can be produced directly in its fluorescing B state, resulting in CN $B \rightarrow X$ emission even at the zero delay time. In addition to the initial spike, we also found that it is necessary to introduce a small time delay to the biexponential rise function, as shown in Fig. 2(A), in order to fit the early part of the transient with an acceptable quality. This time delay, although small, is reproducible and suggests a coherent process prior to the bond breakage. Overall, the transients were fitted to the sum of a delta function at the zero of time and a delayed biexponential rise, both convoluted with the time response function. The initial delay from the fits is 130 ± 30 fs and the time constants for the fast and slow rises are 2.5 ± 0.2 ps and 25 ± 5 ps, respectively. The amplitude ratio for the fast to slow components was found to be about 4.5:1.0 from fitting the long-time transient shown in Fig. 2(C).

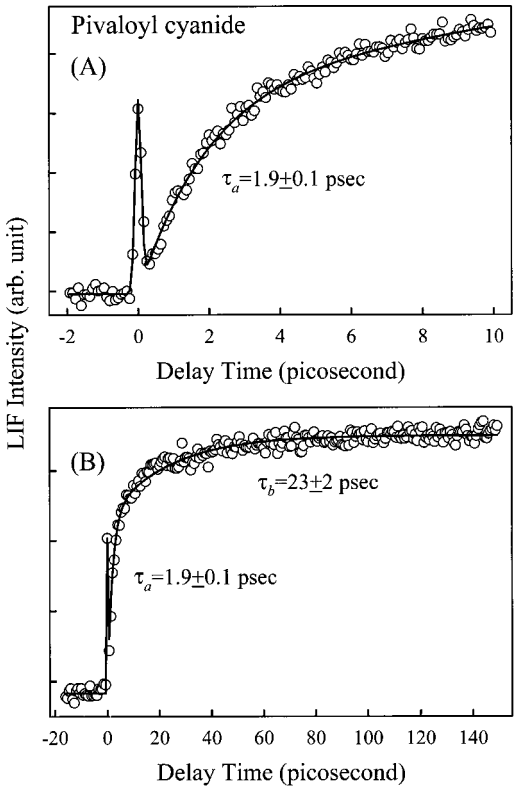

FIG. 4. CN(X) transients following two-photon excitation of pivaloyl cyanide at 388 nm for two different time scales. The two transients have been normalized to the same maximum intensity. The transients presented in this figure are much weaker in the signal size than those shown in Fig. 2, even though the experimental conditions were similar. This forced us to use slightly higher pulse energies, resulting in the larger initial spike at the zero of time. These two transients were fitted in the same way as described in Fig. 2 caption for acetyl cyanide. The rise time constants from the fits are indicated in the figure and the amplitude ratio obtained from fitting the transient in (B) is $A_a:A_b=2:1$.

B. Pivaloyl cyanide

Figure 4 shows the observed transients for the photodissociation of pivaloyl cyanide at two different time scales. The laser irradiance and wavelength dependencies were found to be similar to those observed for acetyl cyanide. Accordingly, we also assigned these transients to the CN(X) fragments produced upon two-photon excitation of pivaloyl cyanide at 388 nm to the ~6.4 eV energy region. However, under similar experimental conditions, i.e., gas pressure and laser irradiance, the transient CN(X) LIF signal resulting from pivaloyl cyanide photodissociation was found to be much weaker than that observed in the acetyl cyanide case. Since the one-photon absorption coefficients are nearly the same for the two compounds at 193 nm,[13] we expected their two-photon transitions are also similar in strength. These suggest a lower CN(X) production yield for the photodissociation of pivaloyl cyanide, consistent with the much lower primary CN elimination branching ($17 \pm 10\%$) reported by Furlan *et al.* for this compound.[13]

The reduction in CN(X) LIF signal forced us to use a slightly higher pump-laser pulse energies (~20 μJ/pulse) in the pivaloyl cyanide case in order to achieve a good signal to noise ratio, resulting in a larger initial spike shown in Fig.

4(A). However, even at the pulse energy used here the laser irradiance dependences are still the same as those found for acetyl cyanide; moreover, the shapes of the transients were found to be invariant, except for the initial spike, even when the pump-laser pulse energy was lowered by a factor of about 3. These pivaloyl cyanide transients were also fitted to delayed biexponential rise functions, as shown in Fig. 4. However, the initial time delay was found to be negligible ($<$50 fs) in this case. The rise times of the fast and slow components from the best fit are 1.9 ± 0.1 ps and 23 ± 0.2 ps, respectively. The fast component becomes slightly faster than that observed for acetyl cyanide, whereas the slow component remains essentially the same if the uncertainties are taken into account. The most notable change is that the amplitude ratio of the fast to slow components changes from 4.5:1.0 for acetyl cyanide to 2.0:1.0 for pivaloyl cyanide, as manifested by the more pronounced biexponential appearance of the pivaloyl cyanide transients.

IV. DISCUSSION

A. Overview

The results and analyses presented above have revealed that, upon two-photon excitation at 388 nm to the ~6.4 eV energy region, both acetyl cyanide and pivaloyl cyanide dissociate to produce ground state CN radicals with a temporal evolution that can be well characterized by delayed biexponential rise functions. These time-resolved data provide important implications to the dissociation dynamics involved. Indeed, the observed ps time scales immediately indicate that the initial excitation at 6.4 eV does not access a repulsive surface directly and the dissociation proceeds via a complex-mode mechanism.

It has been previously proposed that the α-cleavage in acetyl cyanide upon 193 nm (6.4 eV) excitation occurs on the $T_1(n,\pi^*)_{CO}$ surfaces accessed via nonadiabatic transitions from the higher initially prepared states.[11–13] At first glance, our time-resolved data could be interpreted on the basis of this assumption. Briefly, the fast component of ~2 ps could be attributed to the primary C–CN dissociation with its rate determined by the sum of both competing primary C–CN and C–R α-cleavage channels on the T_1 surfaces, where R=CH_3 and C$(CH_3)_3$. The internally hot OCCN fragments resulting from the primary C–R α-cleavage then undergo secondary dissociation, giving rise to the much slower component of ~25 ps. Straightforward as it seems, experimental evidences as well as theoretical considerations discussed below have led us to dismiss this simple T_1 dissociation mechanism. The main reason is that the OCCN radical is a rather stable species with a calculated OC–CN bond energy of 126 kJ/mol (Refs. 11, 12, 15) and an experimentally determined dissociation barrier of $\leqslant$160 kJ/mol.[24] For the primary CH_3 elimination in acetyl cyanide at 6.4 eV, the energy available for partitioning into different degrees of freedom of the fragments is about 260 kJ/mol. However, it is well known that an exit barrier of ~50–60 kJ/mol exists on the T_1 surface for the α-cleavage in simple aliphatic carbonyls.[25,26] Assuming the majority of this exit barrier potential energy is released as product translational energy, it leaves only about 200 kJ/mol of energy to be partitioned into internal modes of the two counterfragments. Statistical theories predict that the OCCN fragments do not acquire enough internal energy to break the bond because both fragments have the same number of internal modes in the case of acetyl cyanide. The OCCN fragments produced in the dissociation of pivaloyl cyanide are expected to have even less internal energy because the large tert-butyl group will take up more energy. In fact, Furlan *et al.*[13] have observed no evidence for the secondary decomposition of the OCCN radicals in their PTS measurements and concluded that it is unimportant ($\leqslant$5%) in all alkyl substituted carbonyl cyanides they have studied, consistent with the above theoretical considerations. Moreover, the simple T_1 dissociation mechanism is expected to produce CN radicals with a long induction period in the ps time scale due to the slow intersystem crossing (ISC) step. This is obviously in contradictory to our observations. The lack of a long induction period in the observed CN growth transients also excludes any forms of consecutive mechanisms involving triplet states only. Thus, we concluded that the photodissociation of acyl cyanides does not follow the simple T_1 dissociation mechanism as other simple aliphatic carbonyls. It is likely that the presence of the unsaturated –CN group gives rise to additional low-lying electronic excited states leading to new photochemical pathways. In the following discussion, we will begin by considering the nature of electronically excited states of acetyl cyanide, we then propose a mechanism to account for our observations. Previous results from other groups will also be discussed on the bases of the proposed mechanism.

B. Excited states of acetyl cyanide

The absorption spectra of acetyl cyanide in the vapor phase from 400 nm to 150 nm have been reported previously.[12–14,27] The first absorption band is weak and is centered at ~310 nm. It has been attributed to the characteristic $n_O\rightarrow\pi^*_{CO}$ transition of carbonyl compounds. Yoon *et al.*[27] have investigated this band in free jets in some detail and have determined its origin at 27 511 cm^{-1}. The onset of the next absorption band, which is also very weak, occurs at ~225 nm.[14] This weak band is then followed by a series of strong absorption bands beginning at ~200 nm.[14]

The state excited near 6.4 eV by one 193 nm photon in previous experiments, or by two 388 nm photons in the present work, has been tentatively assigned to the $^1(n_O,3s)$ Rydberg state,[11,12] in analogy with the absorption of acetone in the similar energy region. Recently, Owrutsky and Baronavski[14] argued that the absorption at 193 nm is due to the $\pi_{CN}\rightarrow\pi^*_{CO}$ transition, based on the *ab initio* calculations using the time-dependent density functional (TDDFT) formalism. The energy of the corresponding state was calculated to be 6.28 eV, consistent with the experimental value of 6.20 eV for the onset of the third absorption band. They also predicted two lower singlet excited states at 3.76 eV and 5.50 eV, which are consistent with the observed first and second absorption bands, respectively.

We have also carried out *ab initio* calculations using the procedures given by Owrutsky and Baronavski[14] for the

TABLE I. Vertical excitation energies and electronic configurations for the first three singlet excited states of acetyl cyanide.

Excited state	Excitation energy (eV)[a]	Dominant electronic configuration	Oscillator strength	E_{obs} (eV)[b]
$S_1(A'')$	3.78	$n_O, \pi^*_{CO/CN}$	0.0005	3.41
$S_2(A'')$	5.48	$a'\pi_{CN}, \pi^*_{CO/CN}$	0.0000	5.51
$S_3(A')$	6.26	$a''\pi_{CN}, \pi^*_{CO/CN}$	0.0478	6.20

[a]Vertical excitation energies calculated at the time-dependent B3P86/aug-cc-pVDZ//MP2/aug-cc-pVDZ level of theory.
[b]Data taken from Ref. 14. Observed energies correspond to long wavelength edges of absorption bands.

acetyl cyanide singlet excited states. Briefly, the ground-state geometry was first optimized at the MP2/aug-cc-pVDZ level of theory and was then used for the single-point TDDFT calculation at the B3P86/aug-cc-pVDZ level of theory. All calculations were performed using the GAUSSIAN 98 program.[19] Table I summarizes our results and the dominant electronic configurations of the first three singlet excited states in the Franck–Condon region. The calculated vertical excitation energies for the first three singlet states are essentially the same as those reported by Owrutsky and Baronavski.[14] However, we note that it is necessary to distinguish the in-plane (a') and out-of-plane (a'') π orbitals localized mostly in the CN moiety (π_{CN}), as shown in Fig. 5. Thus, the excitation at 6.4 eV reaches the S_3 state and is primarily due to promotion of an out-of-plane $a''\pi_{CN}$ electron to the lowest unoccupied molecular orbital (LUMO). We denoted the latter as $\pi^*_{CO/CN}$ because it is significantly delocalized along the O═C–C≡N backbone and has nodal planes bisecting the O–C and C–N bonds (see Fig. 5). The

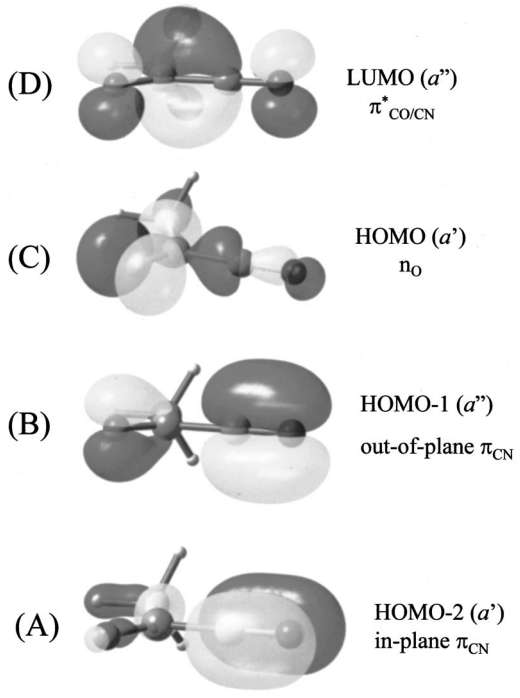

FIG. 5. Isosurface representation of MO's obtained from the DFT calculations at B3LYP/aug-cc-pVDZ level of theory. (A) The in-plane $a'\pi_{CN}$ orbital, (B) the out-of-plane $a''\pi_{CN}$ orbital, (C) the HOMO nonbonding n_O orbital, and (D) the LUMO $\pi^*_{CO/CN}$ orbital.

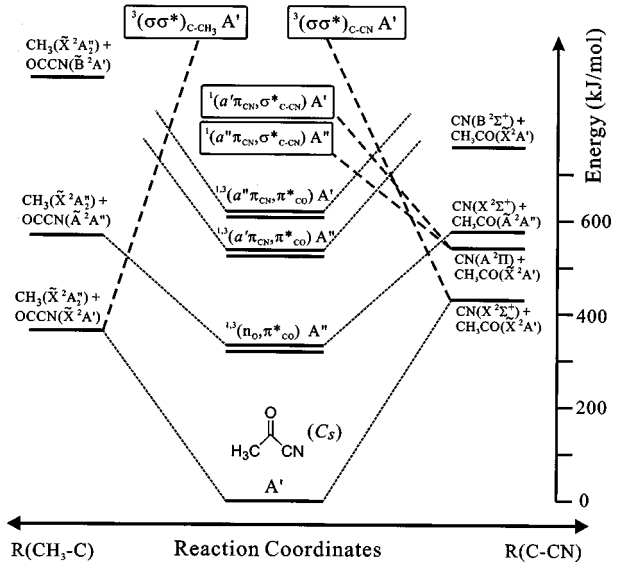

FIG. 6. A configuration correlation diagram of the relevant excited states with the energetically allowed products along both α-cleavage coordinates in acetyl cyanide under C_s symmetry. The solid horizontal lines indicate the best-known energetics and the dashed lines represent the diabatic correlations between various reactant and product configurations.

electronic excitation at 6.4 eV is thus essentially localized along the O═C–C≡N backbone. On the other hand, the S_2 state is due to excitation of an in-plane $a'\pi_{CN}$ electron to the $\pi^*_{CO/CN}$ orbital. The vanishing oscillator strength of the symmetry-allowed $S_0 \rightarrow S_2$ transition simply reflects the very poor spatial overlap between the active orbitals. The corresponding $S_0 \rightarrow S_2$ two-photon transition is also expected to be very weak due to the same reason. Finally, the lowest singlet state, S_1, is due to the characteristic $n_O \rightarrow \pi^*_{CO/CN}$ excitation of carbonyl compounds.

C. Correlation diagrams and potential energy curves

Here, we consider the correlation of the reactant electronically excited states with the energetically allowed products resulting from the C–CN and C–CH_3 α-cleavage reactions. Figure 6 shows a configuration correlation diagram along both α-cleavage paths under C_s symmetry. The diagram was constructed using the valence bond structure descriptions of the reactant and product configurations under diabatic approximation.[28] The dashed lines represent the diabatic correlations between reactant and products in various states. As shown in Fig. 6, the reactant ground-state configuration correlates to the ground-state product pairs along both α-cleavage coordinates. The dominant configuration of S_1, $^1(n_O, \pi^*_{CO/CN})$, correlates diabatically to $CN(X\,^2\Sigma^+) + CH_3CO(A\,^2A'')$ and $CH_3(\tilde{X}\,^2A_2'') + OCCN(\tilde{A}\,^2A'')$ along the C–CN and C–CH_3 dissociation coordinates, respectively. The dominant configurations of S_2 and S_3 correlate diabatically to even more energetic product pairs that are inaccessible to our experiments. Thus, S_1, S_2, and S_3 are all predicted to be bound diabatically along both dissociation coordinates. To become predissociative, these configurations must mix with others having repulsive characteristics along α-bond dissociation coordinates.

One of these repulsive configuration is the triplet $^3(\sigma,\sigma^*)_{C-CN}$ which correlates diabatically to the ground state products along the C–CN α-cleavage coordinate. Note that its corresponding singlet configuration $^1(\sigma,\sigma^*)_{C-CN}$ correlates diabatically to the ion pair products[28] at a much higher energy inaccessible to our experiments. Similarly, there is a $^3(\sigma,\sigma^*)_{C-CH_3}$ configuration correlating diabatically to the ground state products along the C–CH_3 dissociation coordinate. These two can interact with bound triplet configurations, such as $^3(n,\pi^*)_{CO}$, to form adiabatic dissociation barriers. However, as discussed earlier, dissociation on the triplet surfaces alone does not account for our experimental observations. Careful considerations revealed that there are two other configurations, $(a'\pi_{CN},\sigma^*_{C-CN})$ and $(a''\pi_{CN},\sigma^*_{C-CN})$, that are expected to be repulsive along the C–CN dissociation coordinate and correlate diabatically to the excited product pair of $CN(A\,^2\Pi)+CH_3CO(\tilde{X}\,^2A')$, as illustrated in Fig. 6. These two configurations become degenerate at the infinite separation of CN and CH_3CO. They are analogous to the acetyl chloride $^1(n_{Cl},\sigma^*_{C-Cl})$ configuration which plays a key role in its photodissociation reaction.[7,8] In the present case, the –CN group indeed acts as a ''pseudohalogen'' with the π electrons on the CN group playing the role of the nonbonding p electron on the Cl atom in acetyl chloride. These ''additional'' low-lying repulsive configurations arising from the unsaturated CN group can lead to new dissociation pathways that are not present in simple saturated aliphatic ketones. On the other hand, there is no other repulsive configurations, except for the $^3(\sigma,\sigma^*)_{C-CH_3}$ mentioned above, that can correlate diabatically to the accessible excited product pairs along the C–CH_3 dissociation coordinate.

According to these configuration correlations and the best-known energetics,[13,15,27] we applied the noncrossing rule and constructed qualitative potential energy curves, as shown in Fig. 7, along both α-cleavage coordinates for all relevant states. The vertical excitation energies of the repulsive configurations mentioned above are all much higher in energy than the first three bound excited configurations. Topological considerations suggest that their diabatic surfaces must intersect along the α-C–C dissociation coordinates, as illustrated in Fig. 7. Under C_S symmetry, the repulsive $(a''\pi_{CN},\sigma^*_{C-CN})$ configurations is of A'' symmetry, whereas the $(a'\pi_{CN},\sigma^*_{C-CN})$, $(\sigma,\sigma^*)_{C-CN}$, $(\sigma,\sigma^*)_{C-CH_3}$ configurations are all of A' symmetry. For the $^1(a''\pi_{CN},\sigma^*_{C-CN})$ repulsive configuration the crossings with the $^1(n_O,\pi^*_{CO})$ and $^1(a'\pi_{CN},\pi^*_{CO})$ configurations are avoided due to the same symmetry. The S_2 adiabatic dissociation path for the C–CN fission results from these two avoided crossings and correlates adiabatically to $CN(X)+CH_3CO(\tilde{A})$, as shown in Fig. 7. Likewise, the S_1 state correlates adiabatically to $CN(A)+CH_3CO(\tilde{X})$ as a result of the interaction between the $^1(a''\pi_{CN},\sigma^*_{C-CN})$ repulsive configuration and the $^1(n_O,\pi^*_{CO})$ configuration. The repulsive $^3(\sigma,\sigma^*)_{C-CN}$ can interact effectively only with triplet configurations, e.g., $^3(n_O,\pi^*_{CO})$. However, since the $^3(n_O,\pi^*_{CO})$ configuration is of A'' symmetry and the $^3(\sigma,\sigma^*)_{C-CN}$ configuration is of A' symmetry in C_S, they can interact only at nonplanar geometries, resulting in a conical intersection which is not shown in Fig. 7 for the sake of graphic clarity. Thus, the T_1 state can correlate adiabatically to the ground state products only when the molecule is distorted from the C_s geometry. A similar scenario is expected for the interaction between the $^3(n_O,\pi^*_{CO})$ and $^3(\sigma,\sigma^*)_{C-CH_3}$ configurations along C–CH_3 dissociation coordinate. The two triplet repulsive configurations can also interact with the higher triplet bound configurations, e.g., those of the T_2 and T_3 states; however, they are probably not as important as T_1 in the dynamics discussed below and therefore are not shown in Fig. 7. The dominant configuration of $S_3(a''\pi_{CN},\pi^*_{CO})$, should also interact with the repulsive configuration $^1(a'\pi_{CN},\sigma^*_{C-CN})$ and correlate adiabatically to $CN(A)+CH_3CO(\tilde{X})$. This is not shown in Fig. 7 because the barrier thus formed is probably higher than the total excitation energy used here and cannot play a role in the fast dynamics being considered here. These qualitative descriptions of the potential energy surfaces are the key to the understanding of photodissociation dynamics in acyl cyanides, as detailed below.

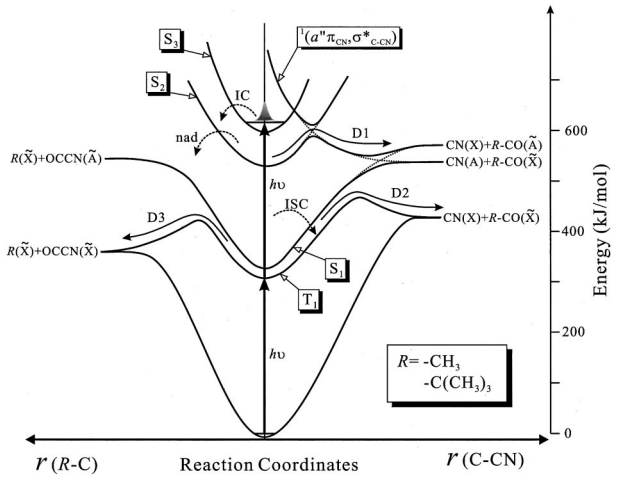

FIG. 7. Schematic potential energy curves of relevant states along the C–CN and R–C dissociation coordinates for the two acyl cyanide compounds. The energetics of minima and asymptotes are drawn to scale according to the best-known literature values for acetyl cyanide. These curves were constructed on the bases of the configuration correlations and noncrossing rule, as discussed in the text. The simplified version of the mechanism (see description in the text) is also illustrated in the diagram using curved arrows. Note that the solid curved arrows represent adiabatic processes occurring along the coordinates specifically indicated by the directions of the arrows, whereas the dashed arrows represent processes that do not necessarily occur along the two coordinates. The locations and directions of these dashed arrows shown in the diagram are somewhat arbitrary.

D. Photodissociation mechanism

In view of all available experimental results and abovementioned theoretical considerations, we have proposed a mechanism for the photodissociation of acyl cyanides in the ~6.4 eV energy region. The mechanism is composed of two discernible stages, corresponding to the two temporal components observed in this work. Although the mechanism is expected to be general for simple acyl cyanides, we will only consider acetyl cyanide here for the sake of simplicity. A discussion for the dissociation of pivaloyl cyanide will be given in the following section.

In the first stage of the reaction, the fs two-photon excitation at 388 nm initially prepares a wave packet on the S_3 surface, as depicted in Fig. 7. We propose that this initially prepared wave packet rapidly couples to the S_2 surface via an ultrafast internal conversion. This process probably occurs through a conical intersection region within a few vibrational periods of the excited modes. The initial delay of ~130 fs in the CN product rise observed by us and the <200 fs initial-state decay observed by Owrutsky and Baronavski[14] can be attributed to this ultrafast $S_3 \rightarrow S_2$ internal conversion process. Rapid internal conversion occurring in high-lying excited states has long been recognized[3,28] and many recent fs time-resolved studies have revealed their ultrafast nature.[29–32]

Following the ultrafast internal conversion, ~7700 cm^{-1} vibrational energy is imparted to S_2 (see Sec. IV G) and the dynamics is thereafter determined by the topology of S_2 adiabatic surface and the initial nuclear configurations launched upon internal conversion. The system quickly moves on the S_2 adiabatic surface and dissociates adiabatically to produce "$CN(X)+CH_3CO(\tilde{A})$" via the barrier formed by the avoided crossing between the $^1(a'\pi_{CN},\pi^*_{CO})$ and $^1(a''\pi_{CN},\sigma^*_{C-CN})$ diabates. We attributed the production of fast-rise $CN(X)$ to this adiabatic dissociation process on the S_2 surface. The CH_3 elimination cannot compete at this stage because the S_2 surface correlates adiabatically along the C–CH_3 dissociation coordinate to products that are energetically inaccessible to our experiment. While the system is searching for exit on the S_2 surface, some trajectories can leak to the lower states via competing nonadiabatic transitions at all configurations. These include $S_2 \rightarrow S_1/S_0$ internal conversion and $S_2 \rightarrow T_2/T_1$ intersystem crossing, which could be further followed by subsequent nonadiabatic processes such as $S_1 \rightarrow T_1$ and $T_2 \rightarrow T_1$. It is the combination of all the competing S_2 decay processes, including the adiabatic dissociation, that ultimately determine the S_2 lifetime and the ~2 ps CN rise time of the fast component.

In the second stage of the reaction, the system can undergo dissociation along both α-cleavage coordinates while it is in the lower states (S_1, T_2, T_1, and S_0) as the total energy is above the dissociation limits to the ground-state products. The slower CN rise of ~25 ps is due to the combination of all these lower-state pathways including the above-mentioned subsequent nonadiabatic transitions. Radiative processes are unlikely to be competitive on the time scales under consideration. The mechanism is complicated in the second stage since the time scale of the slow component (25 ps) led us to consider all possible routes including ISC.

Despite its complexity, this mechanism is consistent with the major temporal features we observed, namely, the initial time delay and the two distinct product rise times. Figure 8 summarizes the mechanism using kinetic expressions. Here k_{IC} is the rate coefficient for the $S_3 \rightarrow S_2$ internal conversion that gives rise to the initial delay. The rate coefficient k_{nad} represents the sum of all nonadiabatic transitions, both spin allowed and forbidden, from S_2 to lower states at all configurations. The rate coefficient k_{D1} denotes the adiabatic dissociation on the S_2 surface, which leads to the formation of $CN(X)+CH_3CO(A)$. Note that the appearance rate of CN in

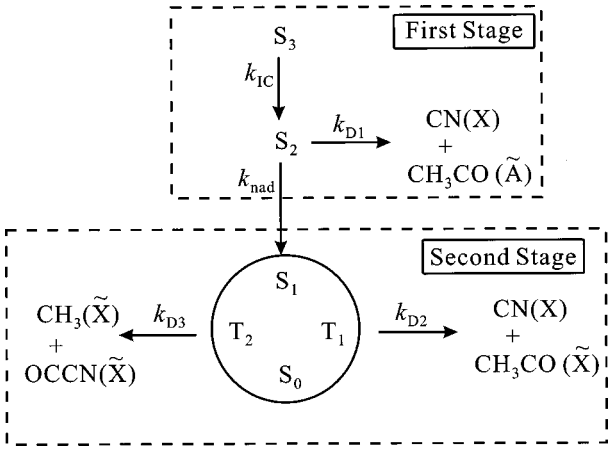

FIG. 8. Kinetic model for the two-stage mechanism described in the text. The dashed boxes represent the imaginary division of the two reaction stages. k_{IC} is the $S_3 \rightarrow S_2$ internal conversion rate coefficient. k_{D1} represents the rate coefficient of the adiabatic dissociation on the S_2 surface. k_{nad} represents the sum of all nonadiabatic transitions rate coefficients from S_2 to lower states. k_{D2} and k_{D3} are the "effective" rate coefficients for the C–CN and C–CH_3 dissociation on the lower state surfaces, respectively.

the first stage of reaction ($1/\tau_a$) is determined by the sum of k_{D1} and k_{nad}, i.e., $1/\tau_a=(k_{D1}+k_{nad})$. Finally, k_{D2} and k_{D3} are the "effective" rate coefficients for the C–CN and C–CH_3 dissociation on the lower-state surfaces, respectively. Among all possible routes in the second stage, the reaction pathway "$S_2 \rightarrow S_1 \rightarrow T_1 \rightarrow \alpha$-cleavage" probably plays the most significant role in producing the slow CN rise. The reason is that the spin-allowed $S_2 \rightarrow S_1$ IC should be reasonably fast to suppress other competing S_2 nonadiabatic decay channels. Furthermore, the dissociation limit of S_1 is high enough to allow the system to be trapped in the S_1 well long enough to couple to the T_1 state. Intersystem crossing from S_1 to T_1 at this high energy is expected to be fast since the density of vibrational levels in both states are extremely high. Once in T_1, the system can rapidly dissociate adiabatically over the much lower barriers near the two conical-intersection regions with the aid of out-of-plane motions. Since the barrier to C–CN dissociation is expected to be higher than the barrier to C–CH_3 dissociation on the T_1 surface (see Sec. IV H), one would predict that the C–CN fission has a lower branching ratio than the C–CH_3 fission, provided that the IVR is much faster. Thus, only a small fraction of the trapped trajectories on the T_1 surface dissociate along the C–CN coordinate to produce $CN(X)+CH_3CO(\tilde{X})$ and give rise to the slow rise of ~25 ps observed in the CN transients. This simplified version of the mechanism is indicated in Fig. 7 with solid arrows. Note that although other relatively unimportant S_2 deactivation channels, such as $S_2 \rightarrow T_1/T_2$ and $S_2 \rightarrow S_0$, are ignored in the simplified mechanism, one should keep in mind that they might still represent an important overall branching.

This slow predissociation mechanism is in direct contradiction to the conclusion of a prompt photodissociation reached by Owrutsky and Baronavski.[14] According to the mechanism proposed above, the ultrafast parent decay (<200 fs) observed by Owrutsky and Baronavski[14] can be attributed to the initial-state decay and does not reflect the

time needed for the excited molecules to fall apart. The nearly instantaneous decay is consistent with the ultrafast $S_3 \rightarrow S_2$ internal conversion proposed above. The transient they observed by monitoring the CH_3CO cation signal is probably dominated by dissociative ionization and the 390 fs decay simply reflects the vibrational and/or rotational relaxation in the S_2 state.[33] A very slow component that appears to be nearly constant following the 390 fs decay is probably the sum of the S_2-state population decay and the neutral $CH_3CO(A)$ product rise. Both components should have the same time constant of 2.5 ps, and thus their sum resembles a nearly constant slow component if they contribute nearly equally.

E. The case of pivaloyl cyanide

The most notable difference between the $CN(X)$ transients observed for the photodissociation of acetyl cyanide and pivaloyl cyanide is that the latter exhibits a more pronounced biexponential-rise behavior and a much smaller total signal. The relative weight of the slow component increases from ~18% for acetyl cyanide to ~33% for pivaloyl cyanide. The rise time of the fast component becomes 1.9 ps for pivaloyl cyanide, slightly faster than the 2.5 ps observed for acetyl cyanide. On the other hand, the slow components in the two cases are almost identical.

The more-weighted slow component observed for pivaloyl cyanide cannot be simply due to a higher CN elimination branching ratio in the second stage of reaction, since, as will be detailed below, the $C-C(CH_3)_3$ dissociation barrier is expected to decrease more than the C–CN dissociation barrier does on going from acetyl cyanide to pivaloyl cyanide (see Sec. IV H). A more consistent interpretation is that in pivaloyal cyanide the branching ratio k_{nad}/k_{D1} increases significantly while the overall S_2 decay rate $k_a = k_{D1} + k_{nad}$ increases only slightly. In such a case, the branching for the adiabatic dissociation on the S_2 surface decreases while the branching for the nonadiabtic transition to the lower states increases, resulting in a larger slow component in the pivaloyl cyanide transients. This interpretation is plausible because, upon replacing the methyl with the much larger tert-butyl group, the adiabatic dissociation rate (k_{D1}) is expected to decrease due to the much greater number of vibrational modes; whereas the nonadiabatic decay rate (k_{nad}) is expected to increase as a result of a much higher density of isoenergetic lower-state levels. The changes of the two rate constants compensate each other such that the overall S_2 decay rate, $k_{D1} + k_{nad}$, increases only slightly from 1/2.5 ps^{-1} to 1/2.0 ps^{-1} on going from acetyl cyanide to pivaloyl cyanide. The net result is a more weighted slow component and an overall decrease in the $CN(X)$ production yield, in accordance with our observations of a lower $CN(X)$ signal level and the lower CN yield reported by Furlan *et al.*[13] for the photodissociation of pivaloyl cyanide. This interpretation is supported by the combined analyses discussed below.

F. Comparisons with photofragment translational spectroscopic results

In this section, we relate our time-resolved data with the photofragment translational spectroscopic results reported by Furlan *et al.*[13] on the basis of our mechanism. The center-of-mass translational energy distribution observed by Furlan *et al.*[13] for the excited-state product (stable acetyl radical) channel of the reaction $CH_3C(O)CN \rightarrow CN + CH_3CO$ peaks at ~10 kJ/mol and tails to 43±5 kJ/mol. This distribution is fully consistent with the predicted available energy of 47 kJ/mol for the D1 dissociation channel proposed in our mechanism for the photodissociation of acetyl cyanide at 6.4 eV. This agreement gives a strong support to the mechanism proposed in this work. For pivaloyl cyanide, Furlan *et al.*[13] observed a much broader translational energy distribution which peaks at ~60 kJ/mol and tails to 210±10 kJ/mol for the primary CN elimination reaction. However, they did not separate the two channels in this case. According to our results, the yield ratio for the D1 to D2 channels in pivaloyl cyanide should be 2:1. The higher weight of the D2 channel (33%) in pivaloyl cyanide should increase the overall kinetic energy release because the available energy for the D2 channel is much higher (~196 kJ/mol at 193 nm excitation for pivaloyl cyanide).[13] Although qualitatively consistent, it is not clear whether the combination of D1 and D2 channels at the 2:1 ratio can produce the translational energy distribution they observed.

Furlan *et al.*[13] also reported that the $C-CN:C-CH_3$ primary dissociation branching ratio is about 85:15 for the photodissociation of acetyl cyanide at 193 nm. They also estimated that about 91% of the CN primary elimination leads to the formation of CH_3CO or CN in one of their energetically accessible electronically excited states, while the rest 9% gives rise to ground state products.[13] According to our mechanism, the 91% excited-state product channel can be assigned to the D1 adiabatic dissociation on the S_2 surface and the 9% ground-state product channel to the D2 dissociation. In our experiment the amplitude ratio of the fast to slow components, which is 4.5:1.0 for acetyl cyanide, reflects the branching ratio between the excited-state (D1) and the ground-state (D2) product channels. This means that 82% of the CN fragments are produced through the D1 excited-product channel, in good agreement with the value of 91% reported by Furlan *et al.*[13]

The combination of the $C-CN:C-CH_3$ primary dissociation branching reported by Furlan *et al.*[13] and the fast to slow amplitude ratio of 4.5:1 observed in our experiments suggests that about 70% of the excited acetyl cyanide decays through the D1 channel and about 15% decays through the D2 channel. The remaining 15% then decays through the D3 channel to produced CH_3. In other words, the branching ratio between the two competing S_2 decay channels is $k_{D1}:k_{nad} = 70:30$. Since the rise time for the $CN(X)$ production via the D1 channel is equivalent to the overall decay time of the S_2 state, we have $1/\tau_a = k_{D1} + k_{nad}$, where τ_a is the observed fast-rise time constant. From these two relations, we obtained $\tau_{D1} = 3.6$ ps and $\tau_{nad} = 8.2$ ps for acetyl cyanide.

Furlan *et al.*[13] also found that in the photodissociation of

pivaloyl cyanide CN is produced with a much lower branching of only $17\pm10\%$, whereas the $C(CH_3)_3$ elimination channel represents a branching of $83\pm10\%$. The much lower CN production they observed in this case is consistent with our observation of much weaker transient LIF signal for pivaloyl cyanide. With the same reasoning described above, these results suggest that about 17% of the excited pivaloyl cyanide decays through the D1 and D2 channel to form ground state CN, while the rest of 83% decays through the D3 channel to produce tert-butyl radicals. Although Furlan *et al.* did not report the branching of the excited-state and ground-state product channels in this case, the fast/slow amplitude ratio observed in our experiments indicates that the ratio of the D1 to D2 channels is D1:D2=2:1 for pivaloyl cyanide. The combination of these data suggests that the yields for the D1 and D2 channels are 11.3% and 5.7%, respectively, and the branching ratio between the two competing S_2 decay steps is $k_{D1}:k_{nad}=11.3:88.7$. Again, by combining with the relation of $1/\tau_a=k_{D1}+k_{nad}$, we obtained $\tau_{D1}=18.6$ ps and $\tau_{nad}=2.37$ ps for pivaloyl cyanide.

These analyses clearly suggest that *the loss of preference for the CN elimination in pivaloyl cyanide is simply due to its slower adiabatic dissociation on the S_2 surface and its faster nonadiabatic transition to lower states*. This is reasonable since the greater number of modes present in pivaloyl cyanide is expected to slow down the adiabatic dissociation, as will be detailed below, and enhance the nonadiabatic decay rate. In other words, in pivaloyl cyanide less trajectories go through D1 to produce fast-rise CN, but in the mean time more trajectories go to S_1 and subsequently to T_1 in which C–CN fission is less favorable. The net result is that the total CN(X) yield decreases and the relative weight of the slower component increases on going from acetyl cyanide to pivaloyl cyanide.

G. Apparent non-RRKM dissociation behavior on the S_2 surface

In the above discussion, we have determined the time constants ($1/k_{D1}$) for the adiabatic dissociation on the S_2 surface to be 3.6 ps for acetyl cyanide and 18.6 ps for pivaloyl cyanide. These results indicate that the presence of the large tert-butyl group slows down the adiabatic dissociation on the S_2 surface by a factor of about 5. Note that although the dissociation pathways in the second stage might be more complex than the simplified kinetic model, the derived k_{D1} (and k_{nad}) does not depend on the exact pathways involved in the second stage. Since there is a large difference in the numbers of vibrational modes between these two compounds (18 for acetyl cyanide and 45 for pivaloyl cyanide) and the dissociation proceeds via a complex-mode mechanism, statistical rate theories predict that pivaloyl cyanide should dissociate much slower than acetyl cyanide does. Although our experimental conclusion is in line with this general prediction, it seems that, given the large difference in the numbers of modes, the decrease in the dissociation rates is not quantitatively consistent with the statistical model.

In order to elucidate the nonstatistical nature of the dissociation, we have carried out Rice–Ramsperger–Kassel–Marcus (RRKM) rate calculations for the adiabatic dissociation on the S_2 surface using the expression,[34,35]

$$k_{RRKM}(E)=\frac{N^{\ddagger}(E-E_0)}{h\rho(E)}, \tag{3}$$

where E is the available internal energy in S_2, E_0 is the C–CN dissociation barrier height on the S_2 surface with zero-point energy correction, $N^{\ddagger}$ is the number of energetically accessible states at the transition state, and $\rho(E)$ is the density of reactant states in S_2 at E. The density of states (ρ) and the number of states ($N^{\ddagger}$) were calculated using the Beyer–Swinehart direct state-counting algorithm[36] for harmonic oscillators. The vibrational frequencies of the T_1 minimum and the C–CN dissociation transition state obtained from *ab initio* calculations, which will be described in the next section, were used as an approximation to the S_2 frequencies needed for the state-counting procedures. The internal energy in S_2 was calculated with $E=E_{h\nu}+E_{therm}-E_0$, where $E_{h\nu}$ is the total two-photon excitation energy, E_{therm} is the average thermal vibrational energy at 298 K and E_0 is the $S_2\leftarrow S_0$ transition origin. Since the alkyl substituents are expected to have only a weak influence on the electronic transition localized mainly along the O=C–C≡N backbone, we used the onset of the acetyl cyanide second absorption band at 5.51 eV as the $S_2\leftarrow S_0$ transition origin for both compounds.[14] Indeed, the previously reported absorption spectra for the two compounds are nearly identical in terms of their band positions.[13] E_{therm} at 298 K was estimated by *ab initio* calculations at the B3LYP/6-311+G(d) level of theory. These calculations gave $E=7700\,cm^{-1}$ for acetyl cyanide and $E=8300\,cm^{-1}$ for pivaloyl cyanide.

The barrier height (E_0) on the S_2 surface is not known and it is rather difficult to obtain a reliable prediction by electronic structure calculations. We therefore calculated the RRKM rates for barrier heights within a reasonable range between 1000–7000 cm^{-1}. The upper limit was chosen to be just below the predicted internal energy in the acetyl cyanide S_2 state. The results are shown in Fig. 9 for both compounds. We expect the barrier heights for the CN elimination on the S_2 surface are similar for both acetyl cyanide and pivaloyl cyanide because it has been shown that for a number of alkyl methyl ketones, R–C(O)–CH_3, the barrier heights for the α-cleavage of the CH_3 group are independent of the nature of R and are nearly the same for R=methyl and tert-butyl groups.[1] Moreover, our *ab initio* calculations described in the next section have shown that the barrier heights for CN elimination on the T_1 surface are indeed almost identical for the two compounds. Although we were not able to calculate the barrier height on the S_2 surface, we expect that its substitution dependence of the barrier height is similar to that on the T_1 surface.

As revealed in Fig. 9, the calculated rates strongly depend on the barrier height and are slower for pivaloyl cyanide, as expected. With a barrier height of $\sim4500\,cm^{-1}$ on the S_2 surface, the RRKM rate agrees with the experimental value for acetyl cyanide. Nevertheless, at the same barrier height the theory predicted that pivaloyl cyanide dissociates at a rate about 200 times slower than acetyl cyanide does; yet the experimental results showed a factor of only 5 slower!

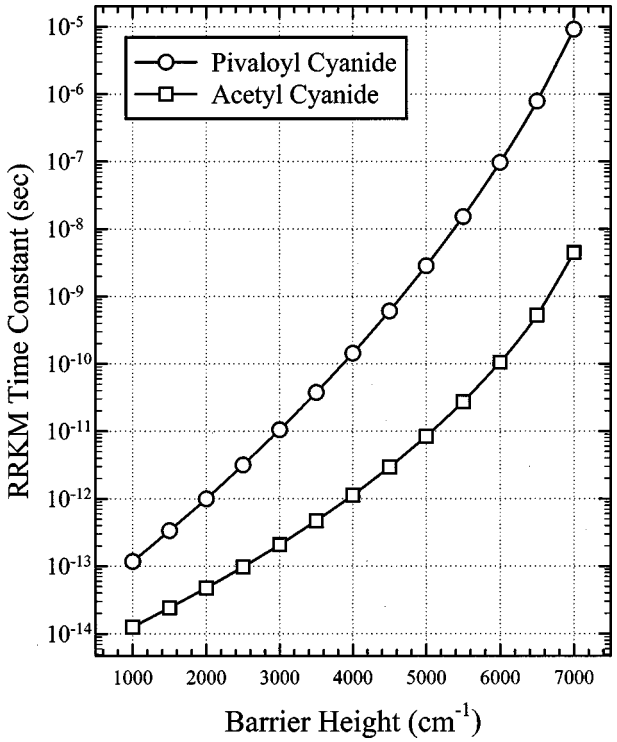

FIG. 9. RRKM time constants ($1/k_{RRKM}$) for the CN elimination reactions of acetyl cyanide (squares) and pivaloyl cyanide (circles) on their S_2 surfaces as a function of barrier heights in the range from 1000 to 7000 cm^{-1}. The rates were calculated with the procedures described in the text. Note that the time constants are plotted on a logarithm scale.

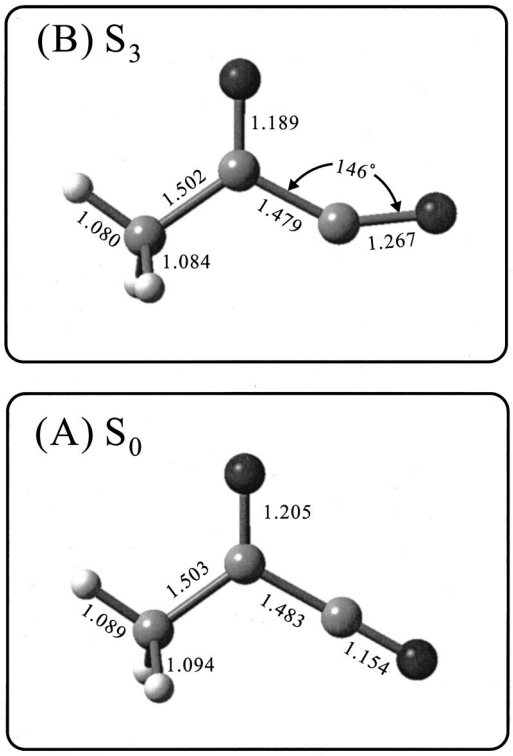

FIG. 10. (A) Equilibrium structure of acetyl cyanide S_0 state optimized at the B3LYP/6-311+G(d) level, and (B) equilibrium structure of acetyl cyanide S_3 state optimized at the CIS/6-311+G(d) level. All bond lengths are in Å.

The ratio between the RRKM rates of the two compounds (acetyl cyanide/pivaloyl cyanide) increases with the barrier height, reaching more than three orders of magnitude at $E_0 = 7000\,cm^{-1}$. On the other hand, the ratios become close to the experimental value for very low barriers ($\sim$1000 cm^{-1}) with predicted time constants in the 10–100 fs range. As will be discussed below, the nature of the electronic transitions involved in the initial preparation implies an initial nonuniform phase space distribution closer to the reaction exit, making the RRKM rates lower than the observed values. Consequently, the barrier height is more likely to be greater than 4500 cm^{-1}. The RRKM theory thus predicts a more than two orders of magnitude decrease in the adiabatic dissociation rates on going from methyl to tert-butyl substitution in acyl cyanides. Clearly, our results revealed a strong deviation from the RRKM predictions.

We speculated that the reason for this non-RRKM behavior is probably due to the nonuniform initial phase space distribution and slow intramolecular vibrational redistribution (IVR).[17] Since the initial electronic excitation to the S_3 ($a''\pi_{CN},\pi^*_{CO}$) state involves mainly the electrons localized in the CN and CO conjugated moieties, the equilibrium geometries of S_3 and S_0 are expected to be quite different along the O═C–C≡N backbone. Consequently, fs excitation to the Franck–Condon region in S_3 would prepare an initial wave packet with its vibrational energy concentrated mostly along the O═C–C≡N backbone. On the other hand, the CH_3–C moiety in acetyl cyanide and the $(CH_3)_3$–C moiety in pivaloyl cyanide are much less perturbed during the initial optical excitation and the subsequent internal conversion because of their similar local geometries in the relevant states. It is plausible that the non-RRKM behavior observed here is simply due to the inefficient coupling between vibrational modes of these two moieties, making the flow of vibrational energy from O═C–C≡N backbone to the alkyl groups slower than the reactions.

To support our speculation, we have carried out *ab initio* calculations for the equilibrium structures of the acetyl cyanide S_0 and S_3 states at the B3LYP/6-311+G(d) and CIS/6-311+G(d) levels of theory, respectively, using the GAUSSIAN 94 program.[18] As the CIS energy is subjected to relatively large errors, the optimized CIS structure should be considered only in the qualitative sense. The optimized structures are schematically depicted in Fig. 10. It is clear that upon electronic excitation to the S_3 state the equilibrium geometry of the O═C–C≡N backbone undergoes a significant structural change, whereas the C–CH_3 moiety remains almost unchanged. Most importantly, the C–N bond length increases from 1.154 Å to 1.267 Å and the C–C–N bond angle change from 180° to 146°. These results are consistent with the qualitative predictions based on the dominant electronic configuration of the S_3 state. Upon electronic excitation to the S_3 state, one of the out-of-plane π bonding electrons in the CN moiety is promoted to the π^* antibonding orbital localized along the O═C–C≡N backbone (see Fig. 5). Thus, it is not surprising that the C–N bond is lengthened significantly. The nonlinear C–C–N geometry suggests that the carbon atom in the CN group adopts an sp^2-like hybrid-

ization due to the removal of one π electron. According to these predicted structures, we expect that upon Franck–Condon excitation to the S_3 state, the C–N stretch and the C–C–N bend are the most excited modes. Since the S_2 is mainly due to the $(a'\pi_{CN},\pi^*_{CO})$ excitation, it can be expected that its equilibrium structures would be slightly different from that of the S_3 along the C–C≡N arm. Conical intersections can exist between S_3 and S_2 along these coordinates, which serve as the so-called "funnels."[3,28] Since these conical intersections are most likely located well above the S_3 minimum, only those initially excited modes are energetically possible to jump to the lower surface. Consequently, the initial vibrational excitations in the C–C≡N arm can be relayed to the lower states (S_2) along the same coordinates via ultrafast internal conversion, provided that the IVR is much slower. Thus, *the initial fs photophysical preparation produces a relatively "hot"* C–C≡N *group and a relatively "cold" alkyl group in* ~100 fs. In other words, the initial activation prepares a phase space distribution more concentrated in a region closer to the reaction exit. The poor coupling between the initially more populated region and the others makes IVR restricted in a finite region near the reaction exit and prevents the system from sampling the entire phase space before bond breaking occurs. The system then redistributes its energy within the restricted phase space region defined by the O=C–C≡N moiety and the dissociation takes place in a time scale of ~2 ps. In such a case, the reaction rates are insensitive to the size of the alkyl group and deviate from the RRKM predictions.

The vibrational level density in S_2 at the available internal energy is $\sim 4.46\times10^4/\text{cm}^{-1}$ for acetyl cyanide and is $\sim 3.11\times10^{10}/\text{cm}^{-1}$ for pivaloyl cyanide, i.e., a more than five orders of magnitude increase. Nevertheless, our results suggest that a great portion of the level-density increase arises from modes that are not strongly coupled to the initially excited modes and that the IVR rates are not proportional to the density of vibrational levels. Similar behaviors have been observed in studies of IVR dynamics using frequency-resolved techniques.[37,38] For example, in studies of a series of compounds $(CX_3)_3C–C\equiv CH$,[39–41] where X=H, D, and F, the spectral line width measurements revealed that the IVR rates for the singly excited acetylenic C–H stretch ($\nu_{CH}=1$) change by a factor of only 5 even though the vibrational state densities span over four orders of magnitude for these three compounds.

It is also worth mentioning here that even though there is a large difference in the C–N bond lengths between the acetyl cyanide S_3 state (1.267 Å) and the free CN radical (1.17 Å), the mechanism is still consistent with the low vibrational excitation of the free CN fragments with a distribution of 0.82:0.15:0.03 for $v=0:1:2$ reported previously.[11,12] This is partly due to the fact that the available energy for the D1 dissociation channel in acetyl cyanide, which is responsible for more than 80% of the CN production, is only barely enough to excite CN $v=2$. Furthermore, the dissociation time of 2.5 ps is long enough for the system to redistribute its energy within the restricted phase space defined by the O=C–C≡N moiety. Thus, the free CN fragments are produced with low vibrational excitation and the product vibrational state distribution appears statistical.[11,12]

H. Dissociation barriers on the T_1 surface

In Sec. IV F, we had estimated the branching ratios between C–CN and C–R (R=methyl or tert-butyl) primary dissociation ($k_{D2}:k_{D3}$) in the second stage of the reaction to be 1:1 for acetyl cyanide and 1:14.5 for pivaloyl cyanide. The equal branching for the two competing α-C–C cleavages in the lower states of acetyl cyanide is surprising, since the general expectation of a lower C–R dissociation barrier on the T_1 surface would predict the C–R bond to break preferentially over the C–CN bond. To elucidate the dissociation dynamics on the T_1 surfaces of the two compounds, we have calculated the barrier heights and performed RRKM rate calculations for the α-C–C bond dissociations.

The procedures for computing the barrier heights are as follows. For acetyl cyanide, we calculated the equilibrium structure for the T_1 minimum at the UB3LYP/6-311+G(d) level of theory. The transition-state structures along the two α-bond dissociation coordinates on the T_1 surface were also calculated at the same level of theory. However, owing to the large tert-butyl group, the structures for the pivaloyl cyanide T_1 minimum and transition states were optimized first at the UB3LYP/6-31G(d) level of theory followed by a single-point energy calculation at the UB3LYP/6-311+G(d) level. The harmonic vibrational frequencies of these optimized structures were then computed at the same levels of theory to characterize the nature of the stationary points and to determine the zero-point energy correction. The method of intrinsic reaction coordinate (IRC) (Ref. 42) was used to confirm that the calculated transition states do correspond to α-C–C bond fission. The energy difference between the transition state and the minimum with zero-point energy correction then gave the barrier heights for the corresponding dissociation coordinates. The RRKM rates were calculated using Eq. (1). The available internal energy in T_1 was calculated with $E=E_{h\nu}+E_{\text{therm}}-E_0(T_1)$, where $E_{h\nu}$ is the total two-photon excitation energy, E_{therm} is the average thermal vibrational energy at 298 K, and $E_0(T_1)$ is the $T_1\leftarrow S_0$ transition origin. Using typical values of S_1-T_1 energy gaps for small aliphatic ketones,[4,26,43] the zero point of T_1 was estimated to be at 2000 cm^{-1} lower than the S_1 zero point.[27] The density of states (ρ) and the number of states ($N^{\ddagger}$) needed for the RRKM calculations were computed using the Beyer–Swinehart direct state-counting algorithm for harmonic oscillators.[36]

In the case of acetyl cyanide, the barrier heights on the T_1 surface with zero-point energy correction were calculated to be 171.2 kJ/mol for the C–CN dissociation and 83.5 kJ/mol for the C–CH_3 dissociation. The latter is much higher than the experimentally determined barrier height of 56 kJ/mol for acetone α-C–C cleavage in its T_1 state.[25] However, since the C–CH_3 bond dissociation energy remains nearly unchanged while the T_1 zero point is lowered by about 35 kJ/mol upon replacing one of the methyl groups with a –CN group in acetone,[44] it is probably not surprising that the T_1 C–CH_3 cleavage barrier height in acetyl cyanide is higher than that in acetone by 27 kJ/mol. The large difference in the

barrier heights along the two α-C–C bond dissociation coordinates immediately suggests that the C–CH_3 bond fission is much more preferable in the T_1 state, provided that the reaction is statistical. Indeed, the RRKM calculations using these calculated parameters gave $\tau_{D2}=23$ ps and $\tau_{D3}=0.36$ ps for acetyl cyanide, which translate to a C–CN:C–CH_3 dissociation branching ratio of ~1:60! This is definitely not consistent with the present experimental results which suggested a ratio of near unity!

In the case of pivaloyl cyanide, the calculations showed that the barrier height for the C–$C(CH_3)_3$ dissociation dramatically decreases to 27 kJ/mol, whereas that for the C–CN dissociation remains almost unchanged at 170 kJ/mol! This is consistent with the general rule in chemistry[45] that the tert-butyl group, $-C(CH_3)_3$, is a better ''leaving group'' than the methyl group and thus should results in a lower barrier to bond dissociation. These results also suggest that the alky substitutions have little or no effect on the C–CN dissociation barrier, giving an additional support to the assumption made in the previous section regarding the non-RRKM dissociation on the S_2 surface. Using these theoretical parameters, the RRKM calculations gave $\tau_{D2}=95$ ns and $\tau_{D3}=0.52$ ps; or a C–CN:C–R dissociation branching ratio of $1:1.8\times10^5$! Although these results deviate from the experimental values by several orders of magnitude, they do indicate that pivaloyl cyanide has a greater lower-state C–R dissociation branching than acetyl cyanide does.

One possible reason causing these large discrepancies between the calculated and experimental branching ratios is that other lower dissociating states, especially T_2, may play an important role in the second stage of the reaction. The difference in the barrier heights along the two α-C–C dissociation coordinates could be smaller on the T_2 surface, making the C–CN and C–R dissociation branching closer. Another possible reason is, again, the incomplete IVR. This is plausible since we have shown in the previous sections that the initially excited modes along C–C≡N arm have poor coupling with the modes localized in the alkyl group. Thus, although IVR is expected to be faster in the T_1 state due to the very high total energy, it is possible that 25 ps is still too short for the system to distribute all vibrational energy statistically throughout the entire phase space, i.e. an incomplete IVR may still exist during the ~25 ps reaction times. If this is the case, the RRKM calculations will underestimate C–CN dissociation rates and overestimate the C–R dissociation rates on the T_1 surface, since the initial vibrational excitation is closer to the exit for C–CN dissociation. Finally, it is worth noting here that even if any dissociating states other than T_1 are involved in producing the slow component, the conclusion reached in the previous section regarding the non-RRKM behavior is still valid, since our derivation did not depend on the exact pathways involved in the second stage of the reaction.

V. CONCLUSIONS

In this study we have measured the temporal evolution of the CN(X) products for the photodissociation of two acyl cyanide compounds in the ~6.4 eV energy region. The observed CN(X) transients are in ps time scales and can be well characterized by delayed biexponential rise functions. These results have provided valuable insights into the photodissociation mechanism of acyl cyanide compounds. We proposed that the photodissociation occurs via two discernible stages that bring about the two temporal components observed in the product transient growth. In the first stage of the reaction, the initially excited S_3 state rapidly jumps to the S_2 state via an ultrafast internal conversion. The S_2 state then subsequently decays through adiabatic dissociation resulting in the fast-rise component in the CN transients. In the second stage of the reaction, other competing S_2 nonadiabatic decay channels bring the system to lower states where α-C–C cleavage along both C–CN and C–R coordinates can occur, giving rise to the slow-rise component of the CN transients.

Evidently, the unsaturated –CN group in acyl cyanides does act like a ''pseudo-halide'' and result in dissociation pathways that are not present in simple aliphatic ketones. The preference of C–CN cleavage in the photodissociation of acetyl cyanide at 193 nm, as reported by other authors,[11–13] is simply a direct consequence of the ''new'' pathway, i.e., the adiabatic dissociation on the S_2 surface. This scenario is very similar to that found in the case of acetyl chloride.[6–8] However, in the present case the branching between C–CN and C–R cleavage is also influenced by the competition between the adiabatic and nonadiabatic dynamics of the S_2 state, since the lower-state dissociation favors the C–R cleavage due to a lower barrier. For acetyl cyanide, the S_2 adiabatic dissociation is more efficient and therefore the overall CN elimination has a much higher branching than the breaking of C–R bond. On the other hand, the S_2 nonadiabatic decay processes are more efficient in pivaloyl cyanide and, therefore, the overall branching for the CN elimination is reduced and the preference for the C–CN breakage is not observed. This study demonstrated that the bond selectivity, i.e., the propensity for C–CN and C–R breakage, can be largely determined by the excited-state dynamics.

In addition to the elucidation of photodissociation mechanism, our results also suggested an apparent non-RRKM behavior in the adiabatic dissociation occurring on the S_2 surface. We proposed that the initial fs excitation and the subsequent ultrafast internal conversion deposit most of the vibrational energy in the C–C≡N moiety. Inefficient coupling between the initially more-excited modes along the C–C≡N arm and those of the alkyl-groups restricts IVR within certain modes and prevents the system from sampling the entire phase space before the reaction completes. This method of nonuniform activation implemented by fs excitation followed by ultrafast photophysical processes may find applications in future studies of unimolecular reactions and IVR dynamics.

ACKNOWLEDGMENTS

This work was supported by the National Science Council of the Republic of China (NSC 89-2113-M-007-014) and by the Ministry of Education of the Republic of China through the Project for Academic Excellence.

[1] M. Reinsch and M. Klessinger, J. Phys. Org. Chem. **3**, 81 (1990).
[2] J. G. Galvert and J. N. Pitts, *Photochemistry* (Wiley, New York, 1966), p. 394.
[3] M. Klessinger and J. Michl, *Excited State and Photochemistry of Organic Molecules* (VCH, New York, 1995), p. 380.
[4] E. K. C. Lee and R. S. Lewis, Adv. Photochem. **12**, 1 (1980).
[5] S. K. Kim, J. Guo, J. Baskin, and A. H. Zewail, J. Phys. Chem. **100**, 9202 (1996).
[6] M. D. Person, P. W. Kash, and L. J. Bulter, J. Phys. Chem. **96**, 2021 (1992).
[7] M. D. Person, P. W. Kash, and L. J. Bulter, J. Chem. Phys. **97**, 355 (1992).
[8] L. J. Butler, Annu. Rev. Phys. Chem. **49**, 125 (1998).
[9] S. S. Hunnicutt, L. D. Waits, and J. A. Guest, J. Phys. Chem. **93**, 5188 (1989).
[10] S. S. Hunnicutt, L. D. Waits, and J. A. Guest, J. Phys. Chem. **95**, 562 (1991).
[11] R. J. Horwitz, J. S. Franciso, and J. A. Guest, J. Phys. Chem. A **101**, 1231 (1997).
[12] S. W. North, A. J. Marr, A. Furlan, and G. E. Hall, J. Phys. Chem. A **101**, 9224 (1997).
[13] A. Furlan, H. A. Scheld, and J. R. Huber, J. Phys. Chem. A **104**, 1920 (2000).
[14] J. C. Owrutsky and A. P. Baronavski, J. Chem. Phys. **111**, 7329 (1999).
[15] J. S. Franciso and R. Liu, J. Chem. Phys. **107**, 3840 (1997).
[16] M. Dantus, M. Rosker, and A. H. Zewail, J. Chem. Phys. **89**, 6128 (1988); A. H. Zewail, *Femtochemistry: Ultrafast Dynamics of the Chemical Bond* (World Scientific, Singapore, 1994), and references therein.
[17] I. R. Lee, W. K. Chen, Y. C. Chung, and P. Y. Cheng, J. Phys. Chem. A **104**, 10595 (2000).
[18] M. J. Frisch, G. W. Trucks, H. B. Schlegel *et al.*, GAUSSIAN 94, Revision E.3 Gaussian, Inc., Pittsburgh, PA, 1995.
[19] M. J. Frisch, G. W. Trucks, H. B. Schlegel *et al.*, GAUSSIAN 98, Revision A.9 Gaussian, Inc., Pittsburgh, PA, 1998.
[20] *Spectroscopic Data*, edited by S. N. Suchard (Plenum, New York, 1975), Vol. 1.
[21] W. M. Jackson, J. Chem. Phys. **61**, 4177 (1974).
[22] C. K. Luk and R. Bersohn, J. Chem. Phys. **58**, 2153 (1973).
[23] V. S. Letokhov, *Laser Photoionization Spectroscopy* (Academic, New York, 1987), Chap. 2.
[24] H. A. Scheld, A. Furlan, and J. R. Huber, J. Chem. Phys. **111**, 923 (1999).
[25] H. Zuckermann, B. Schmitz, and Y. Haas, J. Phys. Chem. **92**, 4835 (1988).
[26] O. Setokuchi, S. Matuzawa, and Y. Schimizu, Chem. Phys. Lett. **284**, 19 (1998).
[27] M. C. Yoon, Y. S. Choi, and S. K. Kim, J. Chem. Phys. **110**, 7185 (1999).
[28] J. Michl and V. Bonačić-Koutecký, *Electronic Aspects of Organic Photochemistry* (Wiley, New York, 1990).
[29] C. C. Hayden and D. W. Chandler, J. Phys. Chem. **99**, 7897 (1995); D. R. Cyr and C. C. Hayden, J. Chem. Phys. **104**, 771 (1996).
[30] W. Radloff, V. Stert, Th. Freudenberg, I. V. Hertel, C. Jouvet, C. Dedonder-Lardeux, and D. Solgadi, Chem. Phys. Lett. **281**, 20 (1997); P. Farmanara, V. Stert, and W. Radloff, *ibid.* **288**, 518 (1998).
[31] V. Blanchet, M. Z. Zgierski, T. Seideman, and A. Stolow, Nature (London) **401**, 52 (1999); V. Blanchet, M. Z. Zgierski, and A. Stolow, J. Chem. Phys. **114**, 1194 (2001).
[32] C. P. Schick, S. D. Carpenter, and P. M. Weber, J. Phys. Chem. A **103**, 10470 (1999).
[33] We believe the 390 fs decay observed by Owrutsky and Baronavski (Ref. 14) reflects the vibrational relaxation dynamics in the S_2 state within the O═C–C≡N moiety. The energy flow to the alkyl group and the complete IVR take much longer times, as discussed in Sec. IV G.
[34] R. A. Marcus, J. Chem. Phys. **20**, 359 (1952).
[35] T. Baer and W. L. Hase, *Unimolecular Reaction Dynamics: Theory and Experiments* (Oxford, New York, 1996).
[36] T. Beyer and D. R. Swinehart, Commun. ACM **16**, 379 (1973).
[37] K. K. Lehmann, G. Scoles, and B. H. Pate, Annu. Rev. Phys. Chem. **45**, 241 (1994), and references therein.
[38] D. J. Nesbitt and R. W. Field, J. Phys. Chem. **100**, 12735 (1996), and references therein.
[39] E. R. Th. Kerstel, K. K. Lehmann, T. F. Mentel, B. H. Pate, and G. Scoles, J. Phys. Chem. **95**, 8282 (1991).
[40] J. E. Gambogi, R. P. L'Esperance, K. K. Lehmann, B. H. Pate, and G. Scoles, J. Chem. Phys. **98**, 1116 (1993).
[41] J. E. Gambogi, K. K. Lehmann, B. H. Pate, G. Scoles, and X. Yang, J. Chem. Phys. **98**, 1748 (1993).
[42] C. Gonzalez and H. B. Schlegel, J. Chem. Phys. **90**, 2154 (1989); J. Phys. Chem. **94**, 5523 (1990).
[43] K. B. Wiberg, R. E. Stratmann, and M. J. Frisch, Chem. Phys. Lett. **297**, 60 (1998).
[44] The C–CH_3 bond dissociation energies are 350 kJ/mol and 359 kJ/mol for acetone and acetyl cyanide, respectively. The S_0–$S_1(0,0)$ transition energy is 30 435 cm^{-1} (364.1 kJ/mol) for acetone and is 27 511 cm^{-1} (329.1 kJ/mol) for acetyl cyanide. Thus, assuming the S_1–T_1 energy gaps are similar for the two compounds, the T_1 zero point of acetyl cyanide is lowered by about 35 kJ/mol from that of acetone.
[45] See, for example, R. T. Morrison and R. N. Boyd, *Organic Chemistry*, 6th ed. (Prentice–Hall, New Jersey, 1992), Chap. 3.